PCCP

Cite this: *Phys. Chem. Chem. Phys.*, 2011, **13**, 9318–9326

www.rsc.org/pccp

PAPER

Amontonian frictional behaviour of nanostructured surfaces†

Georgia A. Pilkington,[a] Esben Thormann,[b] Per M. Claesson,[b] Gareth M. Fuge,[a] Oliver J. L. Fox,[a] Michael N. R. Ashfold,[a] Hannah Leese,[c] Davide Mattia[c] and Wuge H. Briscoe*[a]

Received 24th November 2010, Accepted 11th March 2011
DOI: 10.1039/c0cp02657c

With nanotextured surfaces and interfaces increasingly being encountered in technological and biomedical applications, there is a need for a better understanding of frictional properties involving such surfaces. Here we report friction measurements of several nanostructured surfaces using an Atomic Force Microscope (AFM). These nanostructured surfaces provide well defined model systems on which we have tested the applicability of Amontons' laws of friction. Our results show that Amontonian behaviour is observed with each of the surfaces studied. However, no correlation has been found between measured friction and various surface roughness parameters such as average surface roughness (R_a) and root mean squared (rms) roughness. Instead, we propose that the friction coefficient may be decomposed into two contributions, *i.e.*, $\mu = \mu_0 + \mu_g$, with the intrinsic friction coefficient μ_0 accounting for the chemical nature of the surfaces and the geometric friction coefficient μ_g for the presence of nanotextures. We have found a possible correlation between μ_g and the average local slope of the surface nanotextures.

1. Introduction

With advances in nanotechnology, mechanical devices are becoming smaller and smaller, and with this the surface-to-volume ratio is ever increasing. Concomitantly, friction and other surface related phenomena are predicted to dominate the performance, functionality and durability of future mechanical systems. It is thus important to understand how surfaces interact in tribological processes on the nanoscale.

An effective strategy in modern technologies is to implement textured or structured surfaces to enhance a desired function or property. For instance, synthetic gecko inspired nanostructured adhesives have been developed for use in medical applications[1] and polymeric nanostructures have been utilised to enhance the frictional grip of robotic endoscopes to intestinal tissue.[2] However, our understanding of the frictional behaviour of these nanostructured surfaces is limited.

On a macroscopic scale, our practices of controlling friction have hitherto largely relied on the ancient Amontons' laws of friction.[3] Based on the studies by da Vinci,[4] Amontons[5] and Coulomb,[6] Amontons' laws state that friction is (1) proportional to applied load L; (2) independent of contact area A, and (3) independent of shear velocity V. Together these laws may be summarised by the equation $f_s = \mu L$, where μ is a proportionality constant known as the *friction coefficient*. The question we seek to address here is whether these empirical laws of friction, devised for macroscopic rough surfaces, can be applied to describe the frictional properties of nanostructured surfaces.

In some aspect, this question is not new. It has long been recognised that friction is influenced by asperities that invariably exist on surfaces in real applications. As a result, numerous friction studies have addressed the effect of surface roughness.[7–12] Due to the randomness and irregularity of surface asperities, however, it is difficult to characterise surface roughness and correlate it with observed tribological properties. Consequently, recent research has focused on single asperity friction, facilitated by the development of the AFM[13] and the surface force apparatus (SFA).[14–16] The problem has also been addressed and discussed by advanced simulation methods.[17]

With advances in lithography techniques, it is now possible to design and fabricate surfaces bearing well defined and tuneable nanotextures of sophisticated topography.[18–25] Such surfaces provide model surfaces on which the applicability of Amontons' laws can be tested. Conversely, given the increasing application of these nanostructured surfaces, it is important to understand their tribological properties better. A number of related studies have been carried out recently. A study across silicon (Si) surfaces with micro-grooves (5–20 μm in width and 1.5 μm in height) conducted by Sung *et al.* using a micro-tribotester found that friction

[a] *School of Chemistry, University of Bristol, Cantock's Close, Bristol BS8 1TS, UK. E-mail: wuge.briscoe@bristol.ac.uk*
[b] *Surface and Corrosion Science, Department of Chemistry, Royal Institute of Technology (KTH), Drottning Kristinas Väg 51, SE-100 44 Stockholm, Sweden*
[c] *Department of Chemical Engineering, University of Bath, Bath BA2 7AY, UK*

† Electronic supplementary information (ESI) available. See DOI: 10.1039/c0cp02657c

depended on the groove width and spacing.[26] Marchetto *et al.* found that the presence of such micro-grooves reduced friction as compared with smooth Si surfaces. Upon varying load and velocity they also observed Amontonian frictional behaviours with these micro-grooved Si surfaces.[27] Similarly Choi *et al.* found that friction varied linearly with applied load between highly ordered nickel nanopores (diameter 80–320 nm, spacing 500 nm and depth 300 nm), and a variety of micrometre silica colloidal probes. The magnitude of friction was observed to be higher in the presence of such nanopores as compared with a smooth nickel surface.[28] Mo *et al.* reported that the presence of nanopillars (11 nm in height) on a Si surface reduced both its adhesion and friction with a micrometre sized glass colloidal probe using an AFM.[29] Zhao *et al.*[30] and Burton and Bhushan[31] observed similar effects with nanopillars of various dimensions on gold and poly(methyl methacrylate) (PMMA) surfaces respectively.

From these studies, it is clear that friction is affected by the presence of surface textures. These studies also highlight the possibility of controlling friction with the geometry, distribution, dimensions and material properties of the surface textures. Thus, there is scope for further investigations in which these parameters are varied systematically and correlated with frictional properties. In this study, we have fabricated surfaces with a range of nanostructures including ZnO nanorods, ZnO nanograins, Al_2O_3 nanodomes and nanodiamonds. We have measured friction between these nanostructured surfaces and an AFM tip, and also between ZnO nanorods using an AFM tip functionalised with the nanorods. In this report, we will focus on testing the applicability of Amontons' laws of friction on these nanostructured surfaces. The present results may help guide the design of future devices incorporating nanostructured surfaces. Our ongoing research is also attempting to correlate observed frictional behaviours with two dimensional surface characteristics of the nanostructures. Such information will help to facilitate tuneable friction *via* tailored nanostructures.

2. Experimental

2.1 AFM force measurements

All force measurements were conducted in a fused silica liquid cell in air at room temperature (20 °C) and 30% relative humidity (RH) using a Nanoscope Multimode III AFM (Veeco, Santa Barbara) equipped with a PicoForce unit enabling closed-loop in the normal direction.[32] Uncoated, regular tipped silicon nitride cantilevers (CSC38, A-lever, MikroMasch, Estonia) were used with a typical spring constant of 0.08 N m^{-1} and a radius of tip curvature $R \approx 10$ nm.

Both normal and torsional spring constants (normal, k_N and torsional, k_t) of the cantilevers were determined, prior to use, using the thermal vibration methods by Sader *et al.*[33] and Green *et al.*[34] respectively. The torsional detector sensitivity δ (V rad^{-1}) was determined using the method of tilting the AFM head as suggested by Pettersson *et al.*[35] The vertical and lateral thermal spectra of the cantilevers were recorded using high speed data capture software (Veeco) and their thermal spectra fitted using a MATLAB® script.

Normal forces (adhesion) were measured with a constant approach and a retraction speed of 581 nm s^{-1}, typically at nine positions across each surface, each 2 μm apart. Lateral force (friction) measurements were recorded as a function of both increasing and decreasing load over a scan size of 5 μm and a rate of 1 Hz, corresponding to a shear velocity $V = 10$ μm s^{-1}. To study the effect of varying shear velocity, friction was measured at a particular load with shear rates of 0.1, 1, 5, 10 and 100 Hz.

2.2 Sample preparation

Sample preparation procedures are briefly outlined below, with the details given in the ESI.† The zinc oxide (ZnO) nanograins were grown on Si(100) substrates by a Pulsed Laser Deposition (PLD) method using a ZnO target (Testbourne, 99.99% purity) and an ArF excimer laser (193 nm, Lambda-Physik Compex 201). Zinc oxide nanorod (NR) arrays were subsequently grown on Si(100) substrates using a two stage diffusive pulsed laser deposition (DPLD) method which involved continuing growth on a pre-deposited seedlayer facing away from the target.[36] To functionalise an AFM cantilever tip with ZnO nanorods, the cantilever was substituted in place of the Si substrate in the above process. The nanocrystalline diamond (NCD) films were grown by microwave plasma enhanced chemical vapour deposition (MWPECVD) in a 2.45 GHz reactor on polished Si(100) substrates pre-seeded with 5 nm detonation diamond powder.[37] Typical gas mixtures used for film deposition comprised 1% H_2, 1% CH_4 and 98% X (where X = He, Ne, Ar or Kr, all >99.9% pure). The total gas flow was maintained at 520 standard cm^3 per minute (sccm) in each case but, in order to maintain a stable plasma, it was necessary to use different microwave powers and total gas pressures for each X.[38]

The aluminium oxide nanodomes (40 nm and 70 nm in diameter) were prepared from a two-step anodic oxidation of high purity (99.997%) aluminium foils (Alfa Aesar) using a 0.5 M sulfuric acid or 0.3 M oxalic acid electrolyte, respectively. All the surfaces were characterised by scanning electron microscopy (SEM, JEOL JSM 6330F) and/or by atomic force microscopy (Veeco Multimode with Nanoscope V controller).

3. Results

Fig. 1 shows AFM and SEM images of some of the nanostructured surfaces used in this study. A ZnO nanograin coated Si surface, prepared with an incident laser fluence $F = 15$ J cm^{-2} and a substrate temperature $T_{sub} = 25$ °C, is shown in Fig. 1(a); the average grain diameter is ~60 nm. Different surface coverage and average grain sizes (in the range 40 and 80 nm) were obtained by varying F and/or T_{sub}. The detailed sample characteristics and the associated PLD conditions are summarised in Table S1 of the ESI.†

Fig. 1(b) shows an AFM image of an NCD film on Si, with high surface coverage and an average domain size of 216 nm. Different average crystallite domain sizes, in the range 70–220 nm, could be prepared by use of the different gas mixtures. Fig. 1(c) shows an AFM image of ~70 nm diameter

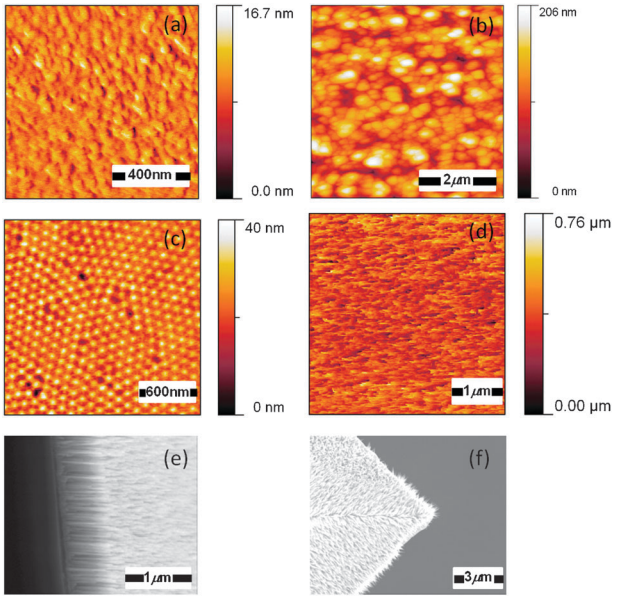

Fig. 1 AFM images acquired with a Si_3N_4 AFM tip ($R \approx 10$ nm) of (a) ZnO nanograins prepared using an incident laser fluence of 22.5 J cm^{-2} at room temperature; (b) CVD nanodiamonds prepared using a He gas mixture; (c) 70 nm Al_2O_3 nano-domes; and (d) ZnO nanorods 600 nm in length and 20 nm in diameter grown on Si. SEM images of ZnO nanorods 225 nm in length on (e) a Si substrate and (f) a Si_3N_4 AFM tip.

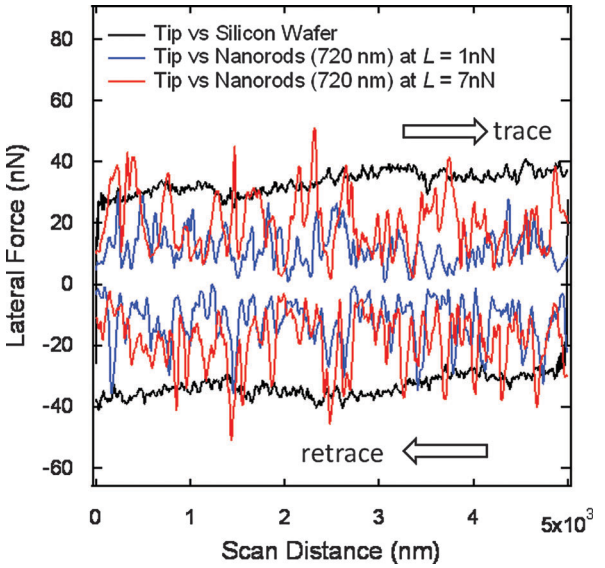

Fig. 2 Examples of raw frictional traces measured between an AFM tip *vs.* ZnO nanorods at different applied loads of 1 nN (blue curve) and 7 nN (red curve) at a scanning velocity of 10 μm s^{-1}. The trace and retrace arrows in the figure indicate friction traces collected from two opposite scan directions. For comparison, the frictional traces for an AFM tip *vs.* a bare silicon wafer (black curves) measured also at 1 nN load and 10 μm s^{-1} are also shown.

aluminium oxide nanodomes. 40 nm nanodomes were also prepared (see ESI†).

Fig. 1(d) shows an AFM image of a ZnO NR array, comprising NRs of length 600 nm and diameter 20 nm, revealing only the upper canopy of the NRs. Such AFM imaging yields useful information on the extent of the inter-digitation of the AFM tip into the NR array, which could corroborate with our friction data below. The full length of the NRs could be revealed using SEM imaging, and a sample SEM image is given in Fig. 1(e), which shows ZnO NRs 225 nm in length taken at a 30° tilt angle. The NR lengths could be varied in the range 225–720 nm by changing the duration of the DPLD process, but their diameters remained constant at ~20 nm. ZnO NRs were also grown on a Si_3N_4 AFM tip by the same method, to a length of 600 nm and similar radius, as shown in Fig. 1(f).

Taken together, the above nanograin, nanodiamond, nano-dome and NR coated surfaces provide a range of nano-structured surfaces of different dimensions, geometries and material properties. It is across these nanostructured surfaces that we made measurements of friction against an AFM tip. In the case of the NRs, measurement was also made against a NR coated AFM tip (*cf.* Fig. 1(f)).

Characteristic of all the nanostructured surfaces investigated, the raw friction trace profiles appear to be dominated by peaks and troughs, rather than smoother sliding as seen on a bare silicon wafer. This is evident from the examples shown in Fig. 2. The height and the density of the peaks in the shear traces varied from sample to sample, and also depended on the applied shear velocity. At low shear velocities, the spacing between the peaks measured for the nanograin, nanodiamond and nanodome samples could be correlated to the spacing of the surface features. However, at higher velocity, the spacing became larger and the peaks became more pronounced, suggesting that the AFM tip may be skipping over some of the surface features. In the case of NRs, such tip skipping was more evident, particularly at higher load, with more pronounced peaks and larger spacing between them, as illustrated in Fig. 2 for shear traces taken at $L = 1$ and 7 nN and 10 μm s^{-1} shear velocity.

To obtain friction forces from these raw traces, two different approaches were taken. Firstly, we took an average of the friction force values of the trace and retrace, as would be done for the smooth shear traces obtained on bare silica surfaces.

Alternatively, we integrated the traces over the scan distance to give the total area enclosed by the trace, which was then normalised by the scan distance. The two approaches yielded friction force values that agreed with each other to within 1%, and should be interpreted as the average lateral force "felt" by the AFM cantilever over the scan distance. We typically averaged ten trace and retrace profiles to obtain one of the friction force data points shown in Fig. 3. Friction traces were also collected at several different areas of each sample.

Fig. 3(a) shows an example of a friction–load curve of an AFM tip *vs.* NCD sample, with ◇ collected upon increasing load (*i.e.*, loading) and ◆ upon decreasing load (*i.e.*, unloading). The tip and the surface are initially not in contact (① in the figure) and become engaged at ②. The applied load is increased and then reversed at ③, until the tip becomes disengaged (*cf.* ⑤). The negative load at ④ indicates an adhesive contact between the tip and the surface. The normal force measurements, in general, showed a small adhesion between the tip and all the surfaces. The measured pull-off forces F_p fall in the

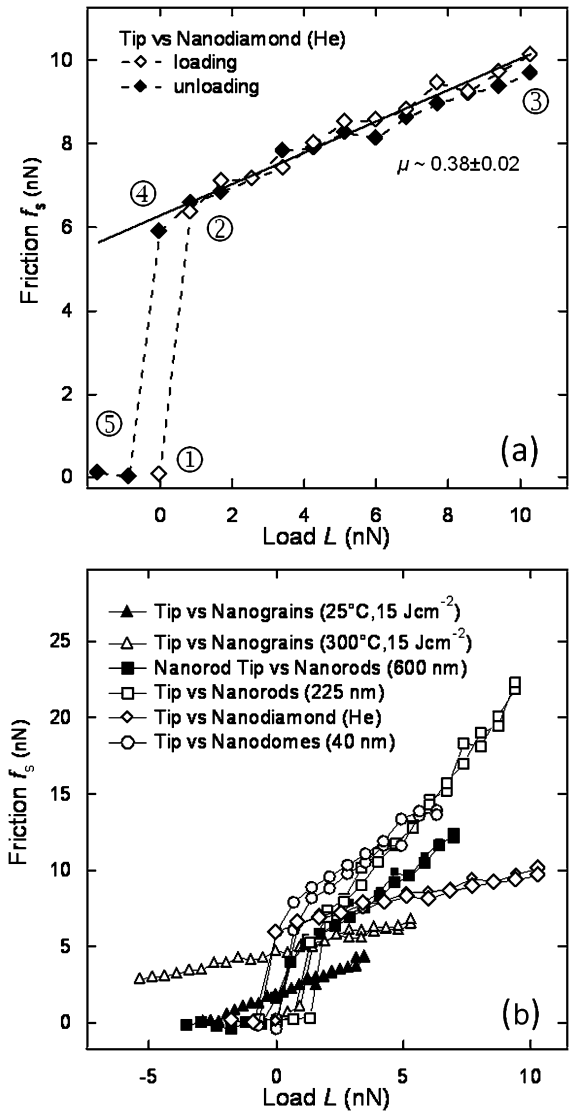

Fig. 3 (a) Friction forces measured with increasing load (loading) and decreasing load (unloading) for an AFM tip against nanodiamonds. The discontinuity upon loading is due to the tip engaging the surface, and upon unloading due to the tip and surface disengaging from the adhesive contact, with events ①–⑤ explained in the text. (b) Comparison of friction measured upon varying applied load across different systems: NR tip *vs.* ZnO nanograins at two different grain sizes (▲ and △); 600 nm ZnO nanorod coated AFM tip *vs.* 600 nm ZnO nanorods (■); NR tip *vs.* 225 nm ZnO nanorods (□); NR tip *vs.* He nanodiamonds (◇); and NR tip *vs.* Al_2O_3 nanodomes (70 nm diameter; ○).

range of ~0–10 nN, as summarised in Table 1. The solid line in Fig. 3(a) is a linear fit to the data points, and the slope of the line $\partial f_s/\partial L$ gives the friction coefficient $\mu \approx 0.38 \pm 0.02$ in this case. Fig. 3(b) plots f_s *vs.* L for all surface types studied, including one example from each system, and is representative of all of our results. A linear f_s–L relationship is evident for all the systems, indicating that Amontons' 1st law is observed. The μ values for all samples studied are listed in Table 1.

We have also measured friction while varying V between 1–200 μm s^{-1}. Generally a mild velocity dependence towards smaller friction with increasing shear velocity was observed for all the samples studied as shown in Fig. 4, despite considerable variations in the shear characteristics in the friction traces registered at different shear velocities (*cf.* Fig. 2).

4. Discussion

Although Amontons' laws have been found to be valid for atomically smooth and macroscopically rough surfaces,[3] their applicability on a nanoscale is less clear. It has been sometimes explicitly stated in the literature (*e.g.*, ref. 43) that "in nanoscale, the well known Amontons' laws of friction are no longer valid". However, in other studies of friction on nanostructured surfaces, Amontons' laws have been found to describe the f_s–L dependence.[27,28] Our observations in Fig. 3 point to a linear f_s–L dependence as predicted by Amontons' laws.

A number of previous studies have attempted to correlate the friction coefficient μ with surface roughness parameters. In Fig. 5(a), the measured μ values for all the systems are plotted against rms roughness, with no correlation found. Similarly, no correlation is found between μ and average roughness R_a. Noting that the shear traces from our nanostructured surfaces are dominated by peaks which could be related to more pronounced surface features (*cf.* Fig. 1), in Fig. 5(b) we also plot μ against the maximum height of the surface roughness as measured with AFM. Again, no clear trend or correlation could be identified.

The validity of Amontons' laws has long been tested on a wide spectrum of surfaces. Most often, these surfaces are either molecularly smooth and thus can be considered in terms of "single asperity contact" as in the case of model SFA studies, or bearing macroscopic random roughness, as in the case of tribological measurements. Our samples with regular, nanosized surface textures fall between these two extremes. Could we invoke various models that have been derived from these studies?

For *single asperity, non-adhesive (or load dominated) contact*, realisable in model friction studies, *e.g.*, using the SFA, a number of phenomenological models have been proposed to explain the linear load dependence of friction. Several such models are based on the Eyring activation model, which states that a kinetic energy barrier ΔE must be overcome to initiate sliding.[44] Both applied shear force f_s and the applied load L would modify ΔE linearly, leading to $f_s \propto L$. In the same vein, the *cobblestone model*, first devised for atomic friction by Tomlinson[45] and later re-articulated by Israelachvili *et al.*,[46] argues that work must be done against an applied load L, as opposing atomic or molecular cobblestones climb from the groove to the summit positions during sliding over an atomic or molecular spacing d, as schematically shown in Fig. 6(a), leading to frictional dissipation linearly dependent on load, *i.e.*, $f_s \approx \varepsilon(\delta/d)L$, where ε is the fraction of energy dissipated in the process.

For *surfaces with macroscopic roughness*, consisting of multiple macroscopic asperities, the explanation of the observation of Amontons' 1st law, $f_s \propto L$, has to deal with two aspects: (1) how the number of contacts, and in turn the total contact area A, between two solid surfaces depend on the load; and (2) how friction between individual macroscopic asperities depends on the load.

Table 1 Pull off force and friction coefficient values for surfaces used

System	Condition	Pull-off force F_p/nN	Average friction coefficient μ
Tip *vs.* silicon	N/A	0.04	1.07
Bulk ZnO[39]	N/A		0.60–0.70
PLD ZnO[39]	N/A		0.15–0.20
Anodic Al_2O_3 nanopores[40]	No pores		0.2
	45 nm		1.2
CVD diamond[41]	29 nm		0.03–0.07
	150 nm		0.55–0.7
Tip *vs.* nanorods	225 nm	3.72	1.77
	450 nm	5.77	10.33[42]
	600 nm	3.37	2.44
	720 nm	2.76	1.66
Tip *vs.* nanograins	7.5 J cm^{-2}	2.7	0.24
	15 J cm^{-2}	2.89	0.66
	22.5 J cm^{-2}	2.83	0.82
Tip *vs.* 300 °C nanograins	7.5 J cm^{-2}	0.02	0.31
	15 J cm^{-2}	0.02	0.38
	22.5 J cm^{-2}	2.77	0.25
Tip *vs.* nanodiamond	Kr	3.38	1.56
	Ar	7.27	0.69
	Ne	7.7	0.38
	He	9.19	0.77
Tip *vs.* nanodomes	40 nm	3.2	0.93
	70 nm	3.66	1.45
Nanorod tip *vs.* nanorods	225 nm	3.06	1.31
	450 nm	6.5	3.47
	600 nm	5.42	1.34
	720 nm	5.03	1.13

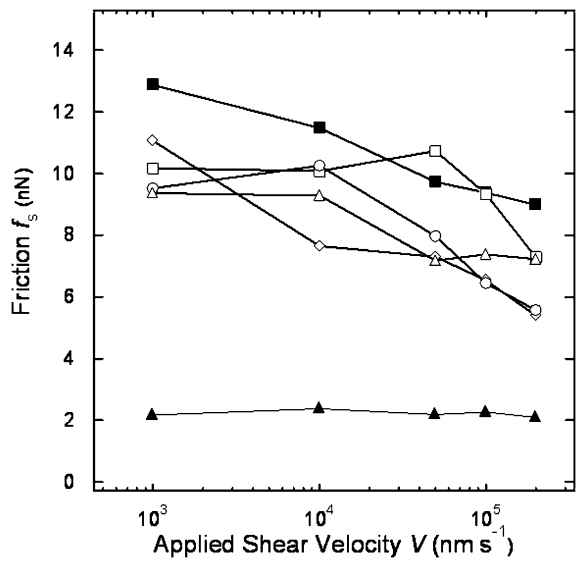

Fig. 4 Comparison of velocity dependence of friction between an AFM tip and different nanostructured surfaces obtained at the applied load $L \approx 1$ nN, with the symbols corresponding to different systems as in Fig. 3.

To address the first of the above two considerations, Bowden and Tabor (BT) observed, by electrical conductivity measurements, that the real contact area A_r between rough metal surfaces was proportional to the load.[47] For plastically deforming surfaces, BT's observations immediately arrived at Amontons' 1st law ($f_s \propto L$). For non-adhering elastic (Hertzian) contact, however, their observations predicted $A_r \propto L^{2/3}$. The apparent inconsistency between BT's observations and Amontons' 1st law was resolved by Archard,[48] who suggested that the number of contacts between surfaces was load dependent and that, upon increasing L, the total contact area between elastic contacts is proportional to L.

Based on Archard's theory, Greenwood and Williamson (GW) proceeded to show that for two rough (non-adhering and elastic) surfaces, with a Gaussian height distribution of spherical asperities, the real contact area would indeed be proportional to the applied load and that Amontons' 1st law, $f_s \propto L$, would thus be observed.

More recently, Berman *et al.* attempted in a *contact value theorem*[49] to explain the load-independence of contact area by making an analogy between the frictional energy dissipation $f_s d$ and energy dissipation $\varepsilon P \Delta V$ during a thermodynamic air compression cycle as schematically shown in Fig. 6(b), where $\Delta V = A_r \delta$ is interpreted as the local volume change in the contact zone due to the vertical deformation δ under the applied L, and ε again is the fraction of dissipated energy and pressure $P = L/A_r$. Equating the above two terms, *i.e.*, $f_s d = \varepsilon P \Delta V$, one obtains $f_s \approx \varepsilon(\delta/d)L$, eliminating A_r and in remarkable agreement with the aforementioned molecular/atomic cobblestone model.

The effect of macroscopic asperities on the μ–L relation has also long been investigated. Euler's interlocking asperity model devised in the 18th century[50] (*cf.* Fig. 6(c)) relates the friction coefficient to the local slope as specified by an inclination angle α, *i.e.*, $\mu = \tan\alpha$. Similarly, in the ratchet mechanism shown schematically in Fig. 6(d), Makinson[51] arrived at a relation $\mu = \mu_0 + \tan\alpha$ after balancing the forces at the contact between an upper surface and an inclined lower asperity of tilt angle α, where $\mu_0 = f_P/f_N$ is defined as the intrinsic friction coefficient between smooth surfaces.

A common feature emerging from these models—devised for molecular or macroscopic asperity contacts—is that the

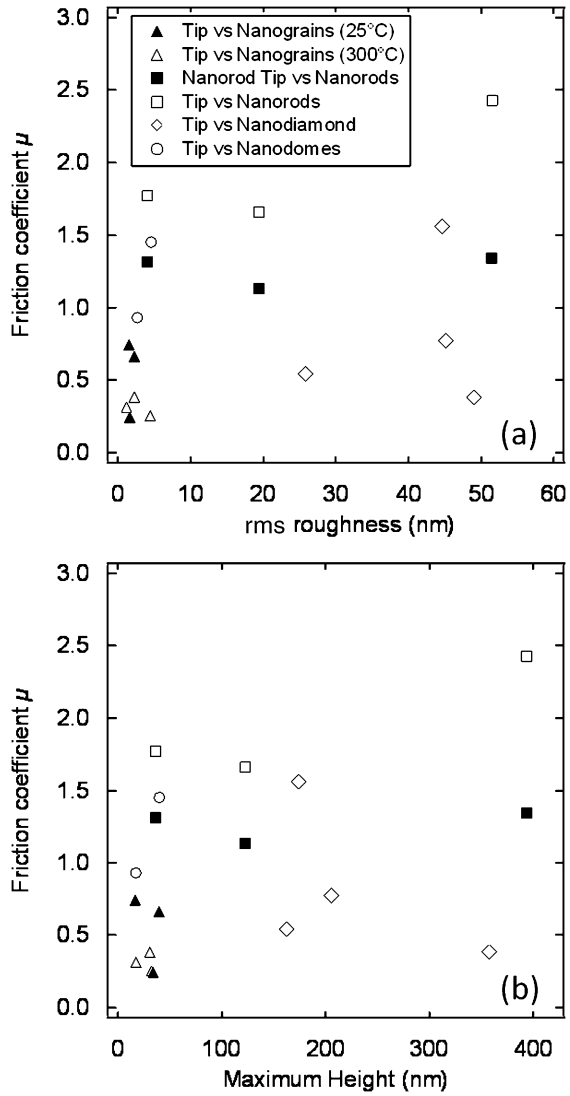

Fig. 5 Comparison of friction coefficients m measured across different systems with respect to (a) measured rms roughness and (b) maximum roughness (height).

friction coefficient μ is directly related to the local asperity slope. Accordingly, we might write for our nanostructured surfaces $\mu = \mu_0 + \mu_g$ where μ_0 is the intrinsic friction coefficient between smooth surfaces and μ_g accounts for the local geometry contribution. We may further write $\mu_g \approx \delta/d$ with δ and d being some vertical and lateral length scales whose ratio defines an *average local slope*. In Fig. 7 we plot μ_g *vs.* δ/d for all the systems studied.

To obtain the μ_g values, we first subtracted the average literature μ_0 values from the measured μ values. For CVD nanodiamonds, $\mu_0 \approx 0.05$–0.1;[41] for Al_2O_3, in the case of nanodomes, $\mu_0 \approx 0.2$[40]; and for PLD ZnO, $\mu_0 \approx 0.15$–0.2.[39] It should be noted that these literature values are not from molecularly smooth surfaces; rather they are measured in the absence of the nanotextures that are present on our surfaces.

Secondly, we had to decide on what δ and d values to use. In the case of δ, we used the mean height (MH) values as registered on all the samples, as listed in the ESI.† For nanodiamonds, nanodomes and ZnO nanograins, this is

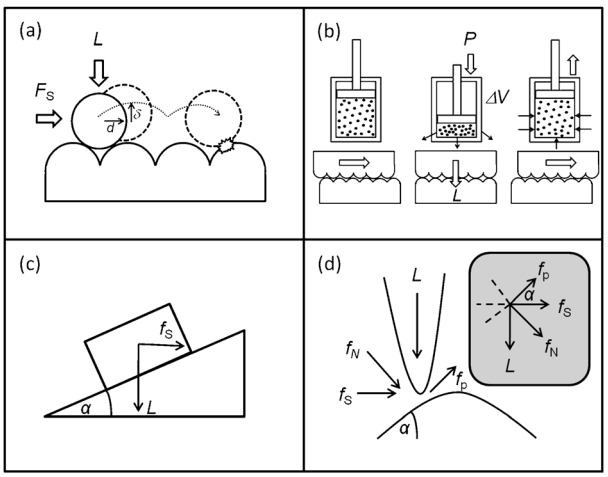

Fig. 6 Schematic representations of (a) the cobblestone model of friction; (b) the contact value theorem; (c) a sliding block on inclined plane in Euler's interlocking asperities model; and (d) an upper surface and a lower surface asperity in the ratchet mechanism.

readily justified, as the MH is the average height that the tip had to climb. However, for ZnO NR samples, the MH values are very different from—much smaller than—the nominal rod heights. The reason for electing to use the MH instead of NR height values for d is that interdigitation between the AFM tip (including the NR coated tip) and the NR array on the substrate is limited. This is evident from Fig. 1(d) where only the "canopy" of the NR array was "seen" by the AFM tip and "felt" in the friction measurement, and thus the MH is what the tip had to climb, not the full rod height.

d was estimated as $d \approx (R + \frac{1}{2}\phi)$ where $R \approx 10$ nm is the radius of the AFM tip (or the radius of the rods in the case of the NR coated AFM tip), and ϕ is specific to each nanostructured surface. For ZnO nanograins, it is the average grain size; for nanodomes, it is the size of the domes as revealed by AFM (*cf.* Fig 1(c)); and for NRs, it is the diameter of the rods, *i.e.*, $\phi \approx 20$ nm. In the case of the nanodiamonds, we used the average domain size as revealed by AFM imaging (*cf.* Fig. 1(b)), although SEM could identify smaller nanocrystallites within the domains as listed in Table S3 in the ESI.† The justification for this is similar to that for using the MH for NR δ values, *i.e.*, it is the domains that the AFM felt and that is thus relevant for the friction measurement.

The solid curve in Fig. 7(a) is an empirical exponential fit to the data points, *i.e.*, $\mu_g = 1.52$–$1.61 \times \exp(-1.12 \times \delta_{MH}/d)$, with the subscript referring to using the MH as δ. The scatter in the data is significant, however, and a power law $\mu_g = -3.11 + 3.97 \times (\delta_{MH}/d)^{0.087}$ also fits the data.[52] We have also attempted to use maximum heights or rms roughness of the nanotextures as δ values instead of the MHs, and the trends are very similar. To demonstrate this, μ_g is plotted against δ_{rms}/d in Fig. 7(b). It is unclear which δ values are the most appropriate to represent the average slope, and we should not over-interpret the physical meaning of the exponential fit or the power law fit. Nonetheless, as compared with the lack of μ–roughness correlation in Fig. 5, Fig. 7 points to a possible correlation between μ_g and the average local slope δ/d. We would also like to note the presence of two apparent regimes in

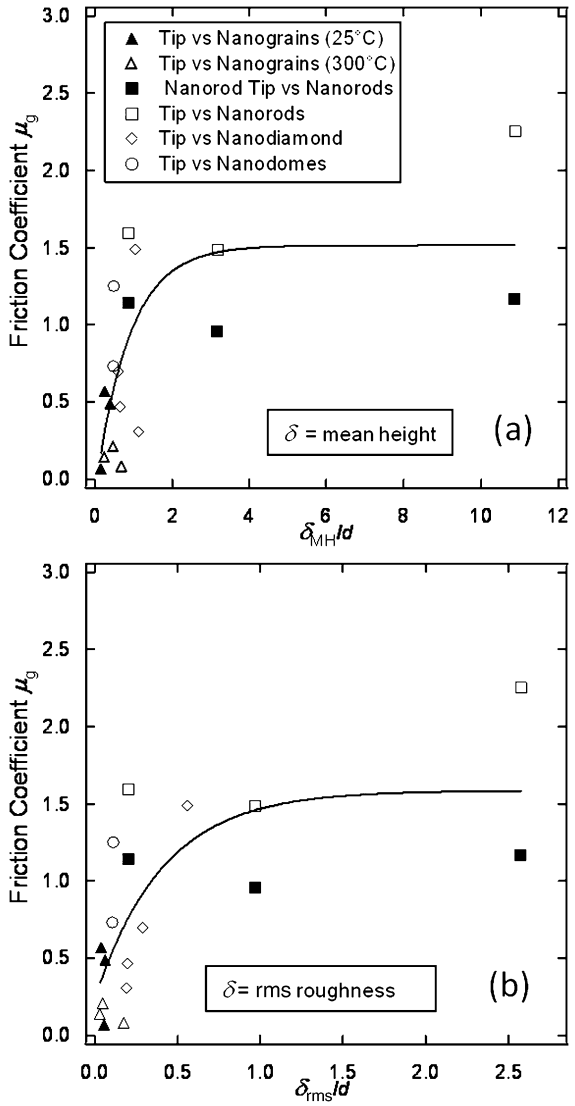

Fig. 7 Comparison of geometric friction coefficients m_g measured across different systems with respect to the ratio δ/d where d is related to the average surface feature size plus radius of the AFM tip and δ is (a) mean surface feature height and (b) root mean squared (rms) roughness (height). The exponential fits (solid curves) to the data points are included to guide the eye.

the μ_g–δ/d correlation. At low δ/d values, μ_g increases rapidly with δ/d (almost linearly). This dependence is consistent with Tomlison's model and Euler's interlocking mechanism which predict such a linear dependence. At higher δ/d values, the μ_g–δ/d dependence appears to plateau. It is conceivable that this second regime, observed for nanotextures with larger vertical dimensions (in our case, nanorods), could be related to the elastic deformations such as bending experienced by the surface asperities. This interpretation is speculative and will be investigated in a further study.

It is worth noting that the applied load in our measurements (up to $\sim$10 nN) is comparable to the registered pull-off or adhesive force, as listed in Table S1 (ESI†). In the case of such adhering surfaces, Derjaguin[53] has suggested that Amontons' 1st law should be modified to read, *i.e.* $f_s = f_{s0} + \mu L$, where f_{s0} is the effective frictional force due to intermolecular adhesive forces. This has been observed in a number of previous works (*e.g.*, ref. 54) and is in line with our observations (*cf.* Fig. 2) where a finite friction value is registered at zero load.

The velocity dependence of friction has been less investigated and a unified picture is yet to emerge. As predicted by Amontons' 3rd law, friction has been found to be largely constant over a wide range of shear velocities on a number of surfaces. For example, Mak and Krim[55] observed a linear friction across full monolayers of both liquid and solid krypton, for a range of sliding speeds, using a quartz-crystal microbalance. Zwörner *et al.* found that friction between silicon AFM tips and different carbon compounds was independent of velocity.[56] However, a logarithmic increase in friction has also been reported across a variety of other surfaces.[57–60] Tao and Bhushan, in a recent study, found the velocity dependence of friction to vary across a range of thin films—reflecting the different mechanisms involved, including adhesion, solid–solid interactions, meniscus bridges, atomic-scale stick slip, impact of the contacts and viscoelastic shear.[61]

As Fig. 4 shows, we observed a slight decrease in friction for all our samples but the nanograins samples. It is fair to comment, however, that the velocity dependence is mild for these nanostructured surfaces over the two and half orders of magnitude velocity range studied. Tambe and Bhushan[60] reported a similar trend, over a comparable velocity range, for an AFM tip *vs.* silicon, and ascribed such a decrease of friction with velocity to reduced meniscus formation. However, their measurement was made at higher relative humidity than ours ($\sim$50% *vs.* 30%[32]). Rather, we ascribe our observed mild decrease in friction with velocity to interactions of the tip with the nanostructured surfaces, *i.e.*, at higher V, the tip might hop and thus skip some of the nanotextures, and thus 'feel' a slightly reduced overall lateral force. We believe that the frictional forces we have measured are dominated by the presence of nanotextures, rather than capillary condensation for the following considerations. (A) Capillary condensation would result in a large hysteresis in the loading–unloading f_s–L curves, as reported by Feiler *et al.*[54] However, no significant hysteresis between loading and unloading is observed in our cases, as evident from Fig. 3. (B) Another previous study[62] noted tilting in the friction force loop at high RH, ascribed to a feature due to capillary condensation. Such tilting is absent from our friction loops as evident from Fig. 2.

5. Summary and outlook

We have measured friction between an AFM tip ($R \approx 10$ nm) and a number of fabricated nanostructured surfaces: ZnO nanograins, ZnO NRs, CVD nanodiamonds and Al_2O_3 nanodomes. We have also functionalised an AFM tip with ZnO NRs and measured its friction with NR coated surfaces. The shear characteristics as registered by raw frictional traces (*cf.* Fig. 2) are dominated by irregular friction peaks that could be related to interactions between the tip and the nanotextures. This is rather different from relatively smooth shear traces or regular stick-slip behaviour observed on surfaces without nanotextures. The density and magnitude of these peaks depended on the nature of the surfaces. However, the overriding outcome of our measurements is

that, despite the variations in the shear traces, the frictional forces are found to vary linearly with the applied load, thereby obeying Amontons' 1st law (with a finite friction force at zero load due to adhesive effects also registered). It is also found that friction was rather insensitive to the applied shear velocity.

No direct correlation was found between measured friction coefficients μ and surface roughness parameters (rms roughness or average roughness R_a) or the height of the surface nanotextures. In order to identify the contribution from the presence of nanotextures to the frictional process, we have defined, in addition to the intrinsic friction coefficient μ_0 which accounts for the material property and associated surface chemistry, an effective geometric friction coefficient μ_g, *i.e.*, $\mu = \mu_0 + \mu_g$. We have attempted to examine the correlation between μ_g and the average local slope δ/d related to the topography of the nanotextures. This points to a possible correlation between μ_g and δ/d as shown in Fig. 7. The significance of this correlation is that it is general, regardless of the chemical nature of different surfaces. Such a correlation would be in line with previous suggestions from a number of friction models that friction is correlated to the slope of the local corrugation, molecularly and macroscopically. Further efforts are required to construct better defined model nanostructured surfaces on which the hypothesis of the μ_g–δ/d correlation could be tested and the exact functional form of the correlation could be established.

Acknowledgements

We are indebted to J. Mitchels (University of Bath) for his advice and technical assistance at the early stage of this project. WHB would like to thank R. Yates and A. Riches at Procter and Gamble (P&G) Reading Innovation Centre for their interest in this project and for a Nanoscience Scholarship awarded to GAP. Financial support from the Engineering and Physical Science Research Council (EPSRC) (MNRA, EP/F048068/1; and WHB, EP/H034862/1) and the European Research Council (ERC) (WHB) is acknowledged. Eamonn Reading is thanked for his comments on our manuscript. PMC and ET acknowledge support from the Swedish Foundation for Strategic Research program "Multi-functional pore arrays in silicon". This project is supported by a Royal Society International Joint Research Project grant (WHB and PMC).

Notes and references

1 A. Mahdavi, L. Ferreira, C. Sundback, J. W. Nichol, E. P. Chan, D. J. D. Carter, C. J. Bettinger, S. Patanavanich, L. Chignozha, E. Ben-Joseph, A. Galakatos, H. Pryor, I. Pomerantseva, P. T. Masiakos, W. Faquin, A. Zumbuehl, S. Hong, J. Borenstein, J. Vacanti, R. Langer and J. M. Karp, *Proc. Natl. Acad. Sci. U. S. A.*, 2008, **105**, 2307–2312.
2 V. P. Elisa Buselli, P. Castrataro, P. Valdastri and A. M. a. P. Dario, *Meas. Sci. Technol.*, 2010, **21**, 105802.
3 J. Gao, W. D. Luedtke, D. Gourdon, M. Ruths, J. N. Israelachvili and U. Landman, *J. Phys. Chem. B*, 2004, **108**, 3410–3425.
4 L. d. Vinci, Codex Atlanticus and other books.
5 G. Amontons, *Mem. Acad. R.*, 1699, 257–282.
6 C. A. Coulomb, *Mem. Math. Phys. Paris*, 1785, 161–342.
7 P. L. Menezes, Kishore and S. V. Kailas, *J. Tribol.*, 2006, **128**, 697–704.
8 N. O. Myers, *Wear*, 1962, **5**, 182–189.
9 D. O. Bello and S. Walton, *Tribol. Int.*, 1987, **20**, 59–65.
10 W. Wieleba, *Wear*, 2002, **252**, 719–729.
11 P. L. Menezes, Kishore, S. V. Kailas and M. S. Bobji, *Tribol. Int.*, 2010, **43**, 897–905.
12 P. L. Menezes, Kishore and S. V. Kailas, *Sadhana*, 2008, **33**, 181–190.
13 R. W. Carpick and M. Salmeron, *Chem. Rev.*, 1997, **97**, 1163–1194.
14 M. Chen, W. H. Briscoe, S. P. Armes and J. Klein, *Science*, 2009, **323**, 1698–1701.
15 W. H. Briscoe, S. Titmuss, F. Tiberg, R. K. Thomas, D. J. McGillivray and J. Klein, *Nature*, 2006, **444**, 191–194.
16 J. Israelachvili, Y. Min, M. Akbulut, A. Alig, G. Carver, W. Greene, K. Kristiansen, E. Meyer, N. Pesika, K. Rosenberg and H. Zeng, *Rep. Prog. Phys.*, 2010, **73**, 036601.
17 Y. F. Mo, K. T. Turner and I. Szlufarska, *Nature*, 2009, **457**, 1116–1119.
18 H. Oizumi, I. Nishiyama, H. Yamanashi, E. Yano, S. Okazaki and J. J. J. Jsap, *Sub-50 nm patterning in EUV lithography*, Business Center Academic Soc Japan, Tokyo, 2000.
19 K. Deguchi, K. Miyoshi, T. Ishii and T. Matsuda, *Jpn. J. Appl. Phys., Part 1*, 1992, **31**, 2954–2958.
20 M. Ringger, H. R. Hidber, R. Schlogl, P. Oelhafen and H. J. Guntherodt, *Appl. Phys. Lett.*, 1985, **46**, 832–834.
21 U. Staufer, R. Wiesendanger, L. Eng, L. Rosenthaler, H. R. Hidber, H. J. Guntherodt and N. Garcia, *Appl. Phys. Lett.*, 1987, **51**, 244–246.
22 D. W. Abraham, H. J. Mamin, E. Ganz and J. Clarke, *IBM J. Res. Dev.*, 1986, **30**, 492–499.
23 J. A. Dagata, J. Schneir, H. H. Harary, C. J. Evans, M. T. Postek and J. Bennett, *Appl. Phys. Lett.*, 1990, **56**, 2001–2003.
24 R. D. Piner, J. Zhu, F. Xu, S. H. Hong and C. A. Mirkin, *Science*, 1999, **283**, 661–663.
25 H. D. Fonseca, M. H. P. Mauricio, C. R. Ponciano and R. Prioli, *Mater. Sci. Eng., B*, 2004, **112**, 194–199.
26 I. H. Sung, H. S. Lee and D. E. Kim, *J. Phys. D: Appl. Phys.*, 2003, **36**, 939–945.
27 D. Marchetto, A. Rota, L. Calabri, G. C. Gazzadi, C. Menozzi and S. Valeri, *Wear*, 2008, **265**, 577–582.
28 D. Choi, S. Kim, S. Lee, D. Kim, K. Lee, H. Park and A. Hwang, *Nanotechnology*, 2008, **19**, 145708.
29 Y. F. Mo, W. J. Zhao, D. M. Huang, F. Zhao and M. W. Bai, *Ultramicroscopy*, 2009, **109**, 247–252.
30 W. J. Zhao, L. P. Wang and Q. J. Xue, *ACS Appl. Mater. Interfaces*, 2010, **2**, 788–794.
31 Z. Burton and B. Bhushan, *Nano Lett.*, 2005, **5**, 1607–1613.
32 Our measurements were performed during a Swedish winter, which was rather dry, facilitating such a low relative humidity consistently over the period of our measurements, which however does (to a certain extent) minimise the effect of capillary condensations.
33 J. E. Sader, J. W. M. Chon and P. Mulvaney, *Rev. Sci. Instrum.*, 1999, **70**, 3967–3969.
34 C. P. Green, H. Lioe, J. P. Cleveland, R. Proksch, P. Mulvaney and J. E. Sader, *Rev. Sci. Instrum.*, 2004, **75**, 1988–1996.
35 T. Pettersson, N. Nordgren and M. W. Rutland, *Rev. Sci. Instrum.*, 2007, **78**, 093702.
36 G. M. Fuge, T. M. S. Holmes and M. N. R. Ashfold, *Chem. Phys. Lett.*, 2009, **479**, 125–127.
37 O. J. L. Fox, J. O. P. Holloway, G. M. Fuge, P. W. May and M. N. R. Ashfold, *Electrospray deposition of diamond nanoparticle nucleation layers for subsequent CVD diamond growth*, in *Diamond Electronics and Bioelectronics—Fundamentals to Applications III*, edited by P. Bergonzo, J. E. Butler, R. B. Jackman, K. P. Loh, M. Nesladek (*Mater. Res. Soc. Symp. Proc.* vol. 1203, Warrendale, PA, 2010), J17–J27.
38 O. J. L. Fox, J. Ma, P. W. May, M. N. R. Ashfold and Y. A. Mankelevich, *Diamond Relat. Mater.*, 2009, **18**, 750–758.
39 S. V. Prasad, J. J. Nainaparampil and J. S. Zabinski, *J. Mater. Sci. Lett.*, 2000, **19**, 1979–1981.
40 H.-s. Kim, D.-h. Kim, W. Lee, S. J. Cho, J.-H. Hahn and H.-S. Ahn, *Surf. Coat. Technol.*, 2010, **205**, 1431–1437.
41 A. Bogus, I. C. Gebeshuber, A. Pauschitz, M. Roy and R. Haubner, *Diamond Relat. Mater.*, 2008, **17**, 1998–2004.
42 Suspected sample damage due to high polydispersity in the nanorod height and resultant high friction. This data point has not been included in Fig. 7.

43 R. R. M. Zamora, C. M. Sanchez, F. L. Freire and R. Prioli, *Phys. Status Solidi A*, 2004, **201**, 850–856.
44 H. Eyring, *J. Chem. Phys.*, 1935, **3**, 107–115.
45 G. A. Tomlinson, *Philos. Mag.*, 1929, **7**, 905–939.
46 J. N. Israelachvili, Y. L. Chen and H. Yoshizawa, *J. Adhes. Sci. Technol.*, 1994, **8**, 1231–1249.
47 F. P. Bowden and D. Tabor, *Proc. R. Soc. London, Ser. A*, 1939, **169**, 391–413.
48 J. F. Archard, *J. Phys. D: Appl. Phys.*, 1973, **6**, 289–304.
49 A. Berman, C. Drummond and J. Israelachvili, *Tribol. Lett.*, 1998, **4**, 95–101.
50 L. Euler, *Mem. Acad. Sci. Ber.*, 1748, **4**, 122.
51 K. R. Makinson, *Trans. Faraday Soc.*, 1948, **44**, 279–282.
52 For both of the exponential and power law fits, μ_g would vanish at $\delta_{MH}/d \approx 0.05$–$0.06$. Note that δ_{MH}/d would never reach zero, as even molecularly smooth surfaces would have Å level corrugations.
53 B. Derjaguin, *Kolloid-Z.*, 1934, **69**, 155–164.
54 A. A. Feiler, J. Stiernstedt, K. Theander, P. Jenkins and M. W. Rutland, *Langmuir*, 2007, **23**, 517–522.
55 C. Mak and J. Krim, *Phys. Rev. B: Condens. Matter*, 1998, **58**, 5157–5159.
56 O. Zwörner, H. Holscher, U. D. Schwarz and R. Wiesendanger, *Appl. Phys. A: Mater. Sci. Process.*, 1998, **66**, S263–S267.
57 T. Bouhacina, J. P. Aime, S. Gauthier, D. Michel and V. Heroguez, *Phys. Rev. B: Condens. Matter*, 1997, **56**, 7694–7703.
58 E. Gnecco, R. Bennewitz, T. Gyalog, C. Loppacher, M. Bammerlin, E. Meyer and H. J. Guntherodt, *Phys. Rev. B: Condens. Matter*, 2000, **84**, 1172–1175.
59 R. Prioli, A. M. F. Rivas, F. L. Freire and A. O. Caride, *Appl. Phys. A: Mater. Sci. Process.*, 2003, **76**, 565–569.
60 N. S. Tambe and B. Bhushan, *Nanotechnology*, 2005, **16**, 2309–2324.
61 Z. Tao and B. Bhushan, *J. Vac. Sci. Technol., A*, 2007, **25**, 1267–1274.
62 K. B. Jinesh and J. W. M. Frenken, *Phys. Rev. Lett.*, 2006, **96**, 166103.

